Check for updates

Efficient synthesis of 5-ethoxymethylfurfural from biomass-derived 5-hydroxymethylfurfural over sulfonated organic polymer catalyst

Yanping Xiang, Sha Wen, Yi Tian, Kangyu Zhao, Dongwen Guo, Feng Cheng, Qiong Xu, Xianxiang Liu [ID] * and Dulin Yin

Herein, we investigated catalytic potential of a functionalized porous organic polymer bearing sulfonic acid groups (PDVTA-SO$_3$H) to the etherification of 5-hydroxymethylfurfural (HMF) to 5-ethoxymethylfurfural (EMF) under solvent-free conditions. The PDVTA-SO$_3$H material was synthesized *via* post-synthetic sulfonation of the porous co-polymer poly-divinylbenzene-*co*-triallylamine by chlorosulfonic acid. The physicochemical properties of the PDVTA-SO$_3$H were characterized by FT-IR, SEM, TG-DTG, and N$_2$ adsorption isotherm techniques. PDVTA-SO$_3$H had high specific surface area (591 m^2 g^{-1}) and high density of −SO$_3$H group (2.1 mmol g^{-1}). The reaction conditions were optimized *via* Box−Behnken response surface methodology. Under the optimized conditions, the PDVTA-SO$_3$H catalyst exhibited efficient catalytic activity with 99.8% HMF conversion and 87.5% EMF yield within 30 min at 110 °C. The used PDVTA-SO$_3$H catalyst was readily recovered by filtration and remained active in recycle runs.

1. Introduction

With the inevitable depletion of non-renewable energy sources such as fossil fuels, as well as the increasing demand for energy, the development and utilization of green and renewable new energy sources has become urgent.[1] Abundant renewable biomass is a green and environmentally friendly energy source that is a key alternative to fossil energy sources such as petroleum and coal for the production of chemicals and liquid fuels.[2] In the past several decades, significant effort has been devoted to synthesizing various value-added chemicals from biomass. 5-Hydroxymethylfurfural (HMF) is an important biomass-derived platform chemical[3,4] and a valuable precursor for the synthesis of biofuels and value-added chemicals.[5] Because its marvellous and reactive structure includes an aldehyde group, a hydroxyl group, and a furan ring, HMF can be further transformed into products such as 2,5-furandicarboxylic acid, 2,5-dimethylfuran, γ-valerolactone, and *n*-butyl levulinate.[6,7]

An etherified product of HMF, 5-ethoxymethylfurfural (EMF), has been identified as a potential nest-generation biodiesel candidate to improve and replace current petroleum-based fuels[8] because of its high miscibility in diesel fuel. Its high energy density (8.7 kW h L^{-1}) is comparable with that of standard gasoline (8.8 kW h L^{-1}) and diesel fuel (9.7 kW h L^{-1}), and is significantly higher than that of the well-known biofuel

National & Local Joint Engineering Laboratory for New Petro-chemical Materials and Fine Utilization of Resources, Key Laboratory of the Assembly and Application of Organic Functional Molecules of Hunan Province, College of Chemistry and Chemical Engineering, Hunan Normal University, Changsha 410081, P. R. China. E-mail: lxx@hunnu.edu.cn

bioethanol (6.1 kW h L^{-1}).[9] The use of EMF also decreases the release of contaminants such as soot, SO$_x$, and NO$_x$ in engine tests when compared with the use of traditional transportation fuels.[10] Furthermore, ethyl levulinate (EL), a by-product formed during the EMF production process, also has significant biodiesel characteristics.[11] Therefore, the synthesis of EMF from biomass-derived feedstock represents a promising strategy for the effective utilization of renewable biomass resources for biofuels.

Several catalytic routes have been developed to date for the synthesis of EMF from carbohydrates or biomass.[12] For example, Wang *et al.*[13] reported that a 55.7% yield of EMF was obtained from fructose with sulfonic acid functionalized ordered mesoporous carbon (OMC-SO$_3$H) as a catalyst after 24 h at 140 °C. Dai *et al.*[14] employed a double-hydrogen-bonded sulfonated polymer catalyst (D-SPC) at 140 °C, and EMF was obtained from fructose in a 68.8% yield within 18 h. Other catalysts such as deep eutectic solvents,[15] [BMIM][HSO$_4$],[16] and Ar-SO$_3$H-SBA-15 (ref. [17]) have also been studied for the synthesis of EMF from hexose. While converting hexose to EMF has the advantage of being a low cost, one-pot process, direct synthesis of EMF from carbohydrates still has some disadvantages, such as a long reaction time, high catalyst loading, and low EMF yield. The selective synthesis of EMF from HMF is a feasible approach for overcoming those disadvantages because it provides a shorter reaction time, lower catalyst loading, high selectivity, and solvent-free reaction conditions.[18,19]

An acid catalyst is the key parameter for the conversion of biomass to EMF or other platform compounds. Catalysts are generally divided into homogeneous catalysts and heterogeneous catalysts.[20] Homogeneous acid catalysts such as H$_2$SO$_4$

and benzenesulfonic acid, which have high catalytic activity, have traditionally been used to catalyse the conversion of biomass to EMF. However, homogeneous acid catalysts suffer from serious drawbacks such as difficulty in separating the catalyst from the reaction mixture and poor catalyst recycling, as well as equipment corrosion.[21] Heterogeneous catalysts can overcome these disadvantages to a certain extent. They are typically separable, recyclable, more thermally stable, and less corrosive to equipment. Heterogeneous catalysts have been widely used in the conversion of carbohydrates, especially in esterification and etherification reactions, because of their Brønsted acidity and high proton mobility, as well as their ability to accept and release electrons.[22]

Sulfonic acid (SO_3H) functionalized materials have generally been found to be efficient solid acid catalysts for the synthesis of EMF.[23] For example, Amberlyst-15,[24] a strongly acidic sulfonated ion-exchange resin which has been employed for EMF production, shows remarkably high catalytic performance, but these commercial resins are costly and have low thermal stability owing to their fragile organic framework.[25] Sulfonated carbonaceous-based materials with relatively high thermal stability, including sulfonated organic polymer and biomass-derived amorphous carbon, are more eco-friendly and cost effective.[26] Sulfonic acid catalysts, such as magnetic cellulose-derived carbonaceous solid acid ($MCC-SO_3H$),[27] S-PANI-$FeVO_4$,[28] and PU-Cat,[29] are a novel class of solid acid catalysts that have been widely used in the synthesis of EMF in recent years. However, a common problem with these sulfonic acid solids is their low surface area. SO_3H groups in bulk amorphous carbon may not be accessed by the reactants, leading to low catalytic activity. These materials are characterized by high surface area, large uniform pores, high thermal stability, and the capability to control the surface hydrophilic/hydrophobic balance as well as the strength and concentration of acid sites, and therefore are promising catalysts for acid-catalysed reactions such as the synthesis of EMF. More broadly, solid acids with SO_3H acid sites and tuneable surface properties appear to have a large potential for the valorisation of biomass.

A sulfonic acid functionalized organic porous polymer ($PDVTA-SO_3H$) was prepared and applied for the etherification of HMF to EMF. The effects of reaction time, reaction temperature, and catalyst amount on the yield of EMF were investigated first, and the reaction conditions were further optimised by response surface methodology (RSM). The reusability of $PDVTA-SO_3H$ was also evaluated. The results demonstrate that the $PDVTA-SO_3H$ catalysts have great potential for the efficient synthesis of the renewable liquid-fuel EMF.

2. Experimental section

2.1. Materials

HMF (97%), EL (99%), and divinylbenzene (DVB, monomer) were purchased from Shanghai Macklin Biochemical Co., Ltd. EMF (97%) was purchased from Shanghai Aladdin Biochemical Technology Co., Ltd. Triallylamine (TAA, monomer), azobisisobutyronitrile (AIBN, radical initiator), and chlorosulfonic acid were obtained from Sinopharm Chemical Reagent Co., Ltd.

2.2. Preparation of the catalyst

2.2.1. Synthesis of PDVTA. PDVTA was prepared by solvothermal co-polymerization of DVB and TAA according to a known method.[30] In a typical synthesis, 4.28 mL DVB (24 mmol) and 1.05 mL TAA (6 mmol) were added to a 100 mL round-bottom flask, then 50 mL dry acetone was added and the mixture stirred for 30 min under a nitrogen atmosphere. Subsequently, 0.1 g AIBN (0.6 mmol) as a radical polymerization initiator was added to the mixture. The mixture was stirred for 12 h at 40 °C under a nitrogen atmosphere before being autoclaved at 120 °C for 24 h without stirring. The obtained solid was soaked and washed thoroughly with acetone to remove residual chemicals and impurities. The product was dried at 60 °C under vacuum to afford a white powder.

2.2.2. Synthesis of PDVTA-SO₃H. Functionalized PDVTA materials were obtained by a sulfonation process. PDVTA powder (1 g) and 40 mL anhydrous dichloromethane were mixed in a 100 mL three-necked round-bottom flask. The flask was immersed in an ice-water bath and the mixture was continuously stirred at 500 rpm for the duration of the reaction. After dispersing evenly, a mixture of 5 mL chlorosulfonic acid and 10 mL anhydrous dichloromethane was then added slowly and the reaction stirred for 4 h under a nitrogen atmosphere. Ethanol was then slowly added dropwise to the violet slurry until there were no bubbles. Finally, the sulfonic acid functionalized catalyst was filtered, washed several times with ethanol, and vacuum dried at 60 °C overnight.

2.3. Catalyst characterization

FT-IR spectra were obtained on a Thermo Nicolet infrared spectrophotometer using a KBr pellet. Thermogravimetric and differential thermogravimetric (TG/DTG) curves were recorded on a TGA4000-FTIR Frontier Analyzer (Perkin Elmer) with a heating rate of 10 °C min⁻¹ from room temperature to 800 °C under a nitrogen atmosphere. X-ray photoelectron spectroscopy (XPS) was conducted on a Thermo Scientific K-Alpha spectrometer with a monochromatized AlKαX source (1486.6 eV) at a constant analyzer pass energy of 12 eV and 6 mA. Nitrogen sorption isotherms were measured with an ASAP 2460 apparatus (Micromeritics, USA). The specific surface area was calculated using the Brunauer–Emmett–Teller (BET) equation, pore volumes were calculated using the t-plot method, and pore sizes were calculated using the Brunauer–Joyner–Halenda (BJH) method based on the adsorption branch of the isotherms. The morphologies of the samples were investigated by SEM (Carl Zeiss Sigma-HD, Germany). The catalysts were coated with gold before SEM observations.

2.4. Acidity titration

The amount of H⁺ in the PDVTA-SO₃H was determined by acid–base titration with a standardised aq. NaOH solution using phenolphthalein as the indicator. Unlike acidity determination for a common inorganic acid, PDVTA-SO₃H was not dissolved in water. For this analysis, 0.1 g of previously dried PDVTA-SO₃H was stirred in 50 mL of saturated NaCl solution at room
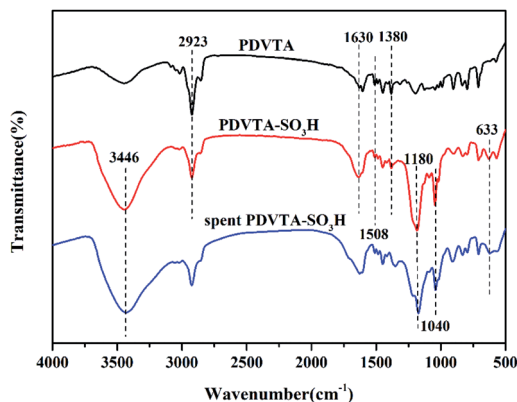
Fig. 1 FT-IR spectra of PDVTA and PDVTA-SO$_3$H.

temperature for 24 h whereupon the H$^+$ was completely released into the solution by exchange with Na$^+$. The released H$_3$O$^+$ was then titrated by a standardised NaOH solution. The titration was stopped when the colourless liquid immediately turned to light red. The amount of H$_3$O$^+$ was equal to the amount of consumed NaOH.

2.5. Synthesis of EMF from HMF

Etherification of EMF from HMF was conducted in a stainless-steel autoclave with a Teflon lining at autogenous pressure.

HMF (126 mg, 1.0 mmol), ethanol (5 mL), and a specified amount of catalyst were added to a 50 mL autoclave reactor. The mixture was magnetically stirred at 300 rpm. The reactor was heated to a specified temperature. After the desired reaction time, the reactor was cooled in an ice-water bath to terminate the reaction, and small aliquots withdrawn from it were passed through a 0.2 μm pore polytetrafluoroethylene membrane (Millipore) filter for GC analysis.

Analysis of EMF and HMF was conducted on a gas chromatograph (Nexis GC-2030) fitted with a capillary column (30 m, 0.25 mm inner diameter, 0.25 μm film thickness), employing a hydrogen carrier gas and a flame ionization detector. The GC parameters were: injection volume 1.0 μL, split ratio 1 : 40, injection port and detector temperatures, 250 °C. The temperature program was set as 100 °C for 1 min, 100–120 °C (10 °C min^{-1}), 120–180 °C (20 °C min^{-1}), 180 °C for 2 min. The chemical species were identified by matching the retention times to known standards.

3.   Results and discussion

3.1.   Characterization of the catalyst

The chemical structures of PDVTA and PDVTA-SO$_3$H were characterized by FT-IR analysis (Fig. 1). Both spectra show bands at 1630 and 1508 cm^{-1} that could be assigned to the C=C stretching vibration, while the absorbance at 2923 cm^{-1} was attributed to the aromatic C–H stretching vibration. The
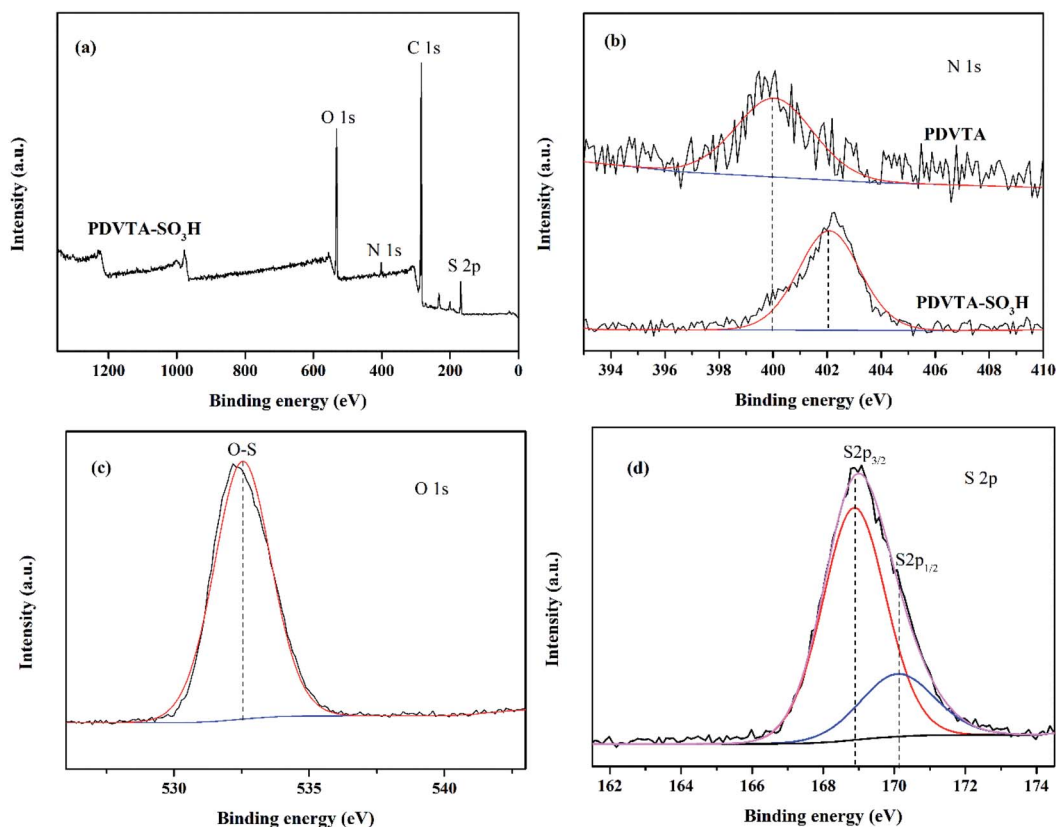

Fig. 2 XPS spectrum of PDVTA and PDVTA-SO$_3$H in the (a) survey, (b) N 1s, (c) O 1s, (d) S 2p.

band at 1380 cm^{-1} originated from the stretching vibration of the C–N groups. For PDVTA-SO$_3$H, a band at approximately 3446 cm^{-1} that is typically assigned to the –O–H stretching vibration of sulfonic groups was observed, and a pair of peaks centred at 1180 and 1040 cm^{-1} were attributed to the SO$_3^-$ stretching and O=S=O stretching vibrations, respectively. The peak at approximately 633 cm^{-1} was attributed to the C–S stretching vibration, demonstrating that the SO$_3$H groups were successfully bonded to the aromatic rings in the polymeric chain after PDVTA was treated with chlorosulfonic acid.

The surface composition and chemical state of the constituent elements of PDVTA and PDVTA-SO$_3$H were confirmed from X-ray photoelectron spectroscopy (XPS). Fig. 2a demonstrates the full surface survey of PDVTA-SO$_3$H, in which the single O 1s, N 1s, C 1s and S 2p signals were clearly observed at around 532.5 eV, 402.0 eV, 284.5 eV and 170.2 eV respectively. As seen from Fig. 2b, the peak centered at 400.0 eV is typically assigned to C–N of graphitic N. After sulfonation, the shift of N 1s XPS peaks to 402.0 eV can be also attributed to the added of –SO$_3$H that changes the original electronic environment of graphitic N. In addition, the observed O 1s spectra showing strong peak at 532.5 eV could be ascribed to O–S in the sulfonic group (Fig. 2c). For the S 2p XPS peaks of PDVTA-SO$_3$H sample, the peaks centered at 168.9 and 170.2 eV were ascribable to grafted –SO$_3$H groups (Fig. 2d). The above results further confirmed that –SO$_3$H groups were firmly bonded to the polymer framework. These results indicated that this PDVTA materials were successfully functionalized with –SO$_3$H groups.

The porosity and surface characteristics of the as-prepared PDVTA and PDVTA-SO$_3$H were derived from N$_2$ adsorption–desorption isotherms, and the profiles are presented in Fig. 3. Both PDVTA and PDVTA-SO$_3$H displayed typical IV-type N$_2$ sorption isotherms with a significant hysteresis loop in a wide range of relative pressure (0.45< P/P_0 <0.95), demonstrating their meso porosities. Moreover, a large amount of nitrogen uptake was observed in the low-pressure region (below 0.1 bar). This suggests the existence of appreciable amounts of
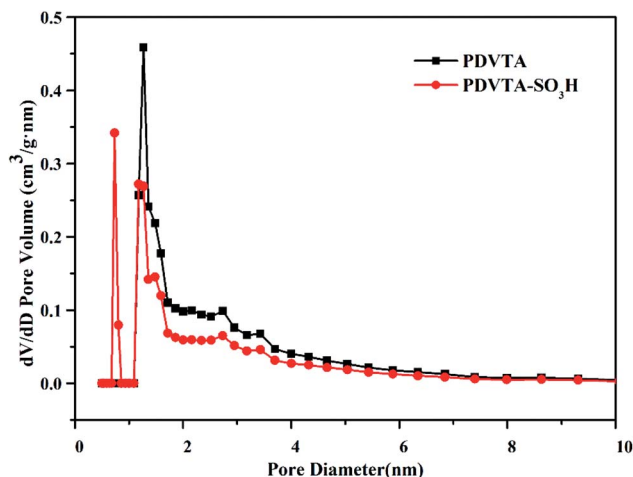

Fig. 4 Pore size distribution of PDVTA and PDVTA-SO$_3$H.

interparticle micropore voids in these organic polymers. Pore size distribution curves were obtained by the BJH method, taking adsorption branches into account (Fig. 4). The materials have considerable microporosity, which is primarily distributed at 0.73 nm. This is a unique property of these materials, and may have a positive impact on the catalytic activity. As listed in Table 1, the parent PDVTA material possessed a high BET surface area and pore volume of 774 m^2 g^{-1} and 0.54 cm^3 g^{-1}, respectively. PDVTA-SO$_3$H exhibits similar adsorption behaviour to PDVTA, including a BET surface area of 591 m^2 g^{-1} and a pore volume of 0.41 cm^3 g^{-1}. Obviously, PDVTA-SO$_3$H has decreased surface area, pore volume, and average pore diameter, indicating the modified functional groups exist in the pores, which is in good agreement with the pore size distribution.

The thermal stability of PDVTA and PDVTA-SO$_3$H were investigated by TG/DTG analysis, and the results are shown in Fig. 5. The weight loss detected below 100 °C was attributed to the removal of adsorbed water and volatile components. From approximately 200–300 °C, the weight loss could be ascribed to desorption of decomposed sulfonic acid groups. The sharp peaks occurring at 430 and 450 °C were attributed to the successive destruction of the PDVTA and PDVTA-SO$_3$H polymer framework, respectively, indicating the thermal stability of the carbon materials slightly increases after acid treatment. Additional weight loss at 650 °C signified the thorough decomposition of the benzene ring building block. The as-prepared PDVTA-based solid acidic catalyst had reliable thermal
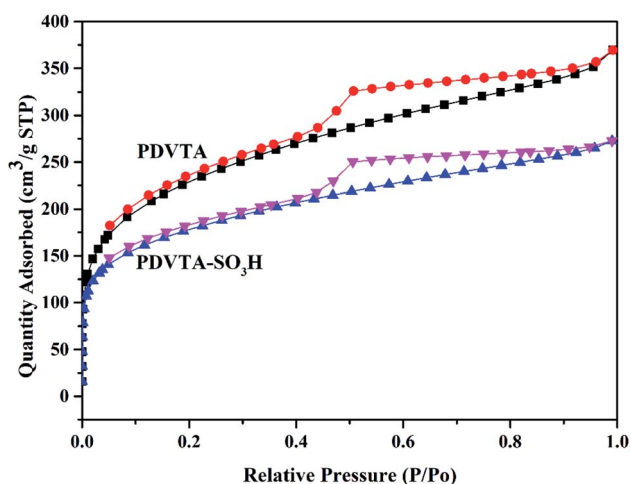

Fig. 3 Nitrogen adsorption–desorption isotherms for the synthesized PDVTA and PDVTA-SO$_3$H.

Table 1 Physicochemical properties of PDVTA and PDVTA-SO$_3$H

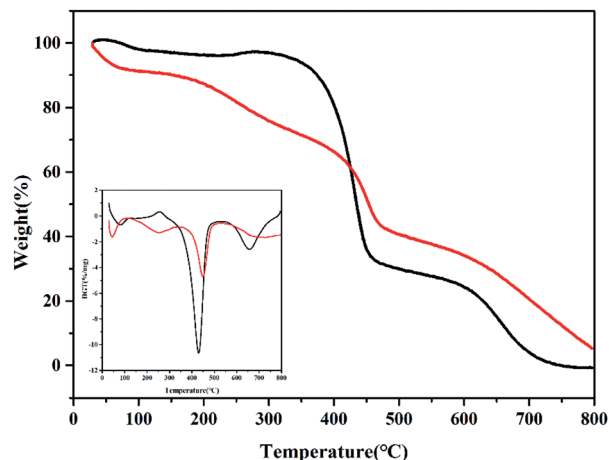| Catalyst	BET surface area/m^2 g^{-1}	Pore volume/ cm^3 g^{-1}	Micropore volume/cm^3 g^{-1}	Pore size/ nm
PDVTA	774	0.54	0.07	3.6
PDVTA-SO$_3$H	591	0.41	0.09	3.4

Fig. 5 TG/DTG curves of PDVTA (black) and PDVTA–SO$_3$H (red).

stability within temperatures below 250 °C, indicating it is sufficiently stable at the reaction temperature required for the conversion of HMF to EMF.

The surface morphologies of the as-prepared PDVTA and PDVTA–SO$_3$H were observed by scanning electron microscopy (Fig. 6). All the PDVTA-based carbon materials were composed of similar irregular amorphous carbon particles within a size range of 10–20 nm and have a flaky or lamellar structure.

3.2. Catalytic performance

The catalytic etherification of HMF to EMF was carried out in an autoclave using heat and autogenous pressure with ethanol as both reactant and reaction medium. The results are listed in Table 2. The major reaction products observed are EMF and EL. EMF is derived from the etherification of HMF *via* acid catalysis, while EL is formed stoichiometrically from the hydration of EMF, as shown in Scheme 1.[31] A control experiment performed without any catalyst showed negligible production of EMF. When catalysed by PDVTA, the HMF conversion was only 22.8% and the EMF yield was only 6.2%. The PDVTA–SO$_3$H catalyst clearly accelerated the conversion of HMF, achieving a high conversion of HMF and an 87.5% yield of EMF. This shows that the incorporation of SO$_3$H into PDVTA facilitated the etherification reaction, leading to EMF as the major product with very high selectivity. Commercially available Amberlyst-15 and the homogeneous sulfonic acid P-TSA were used for comparison with PDVTA–SO$_3$H because they all have an aromatic ring directly attached to the SO$_3$H group. Although the active sulfonic acid sites of these catalysts were similar in nature, the catalytic activity of PDVTA–SO$_3$H was higher than that of Amberlyst-15 and P-TSA. In addition, P-TSA is soluble in ethanol and could not be recycled. The efficient catalytic activity of PDVTA–SO$_3$H was most likely due to the existence of an appropriate pore diameter as well as an appropriate number of Brønsted acid sites. According to the pore size distribution of
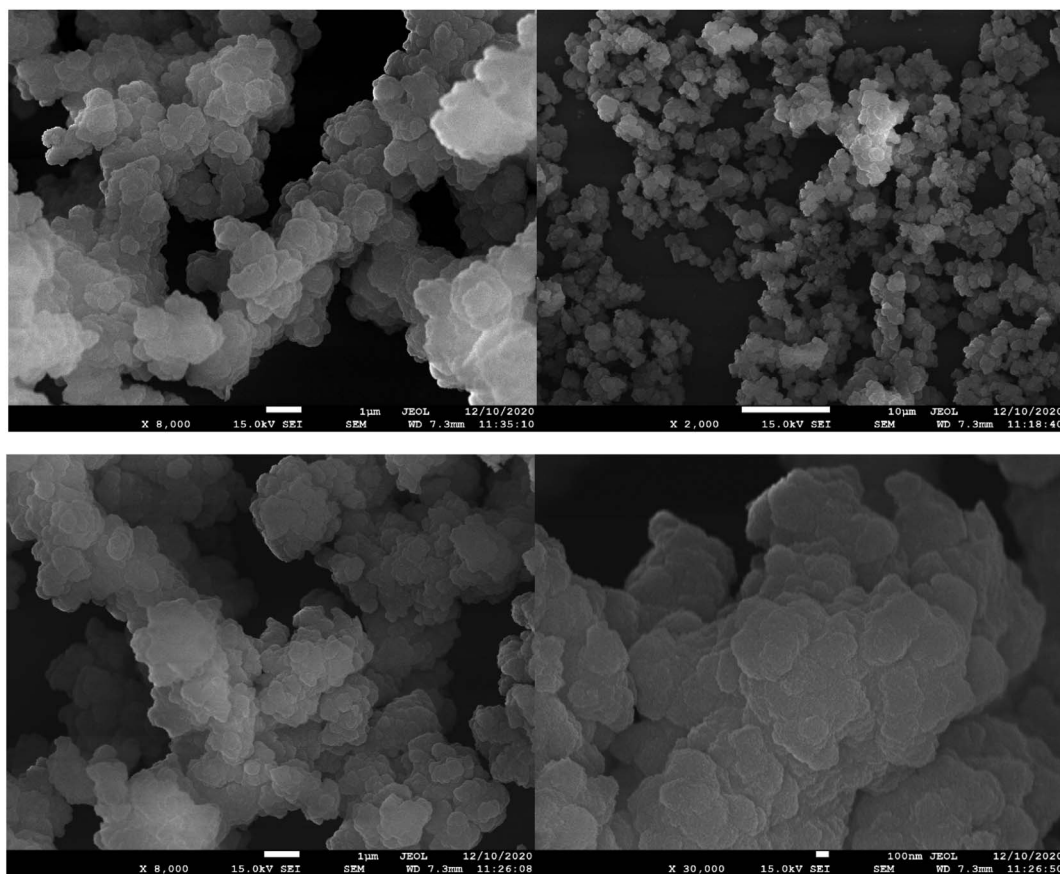

Fig. 6 SEM images of PDVTA and PDVTA–SO$_3$H.

Table 2 Etherification of HMF into EMF over various catalysts[a]

Entry	Catalyst	HMF conv./%	EMF yield/%	EMF sel./%	EL sel./%
1	—	7.0	0.1	2.0	0.7
2	PDVTA	22.8	6.2	27.0	4.5
3	PDVTA-SO$_3$H	99.8	87.5	87.7	12.3
4	P-TSA[a]	99.5	82.9	83.3	16.7
5	Amberlyst-15	85.4	70.8	82.9	7.1

[a] Reaction conditions: HMF (1 mmol, 0.126 g), ethanol (5 mL), and catalyst (42.5 mg), 110 °C, 30 min. [a]Corresponding amount of sulfonic acid.
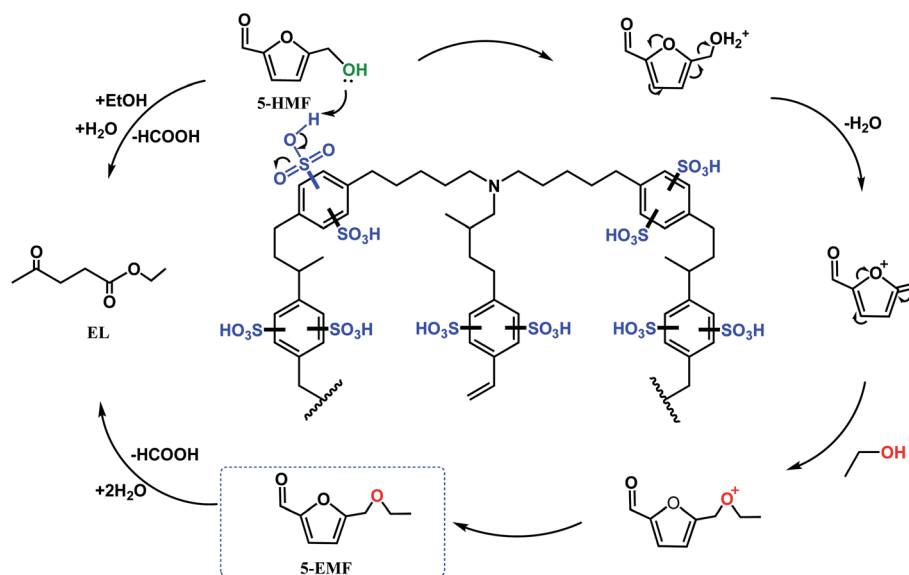
Scheme 1 Reaction mechanism of the PDVTA-SO$_3$H catalysed conversion of HMF to EMF and EL in ethanol.

PDVTA-SO$_3$H, it can be seen that a portion of the pores inside the catalyst are 0.73 nm in diameter, which is larger than the HMF molecular size of 0.71 nm and less than that of EMF.[31] This pore size is conducive to stabilizing the synthesis of EMF by reducing the probability of EMF further transforming into the by-product EL. This suggests acid catalysis occurs both on the surface and inside of the catalyst.

3.3. Optimisation of EMF production

3.3.1. Experimental design. A RSM with a Box–Behnken design was adopted to optimise the PDVTA-SO$_3$H-catalysed EMF production from HMF when multifactorial reaction variables were fully considered.[32] The Box–Behnken design with three variables (reaction time, reaction temperature, and catalyst dosage) was applied according to the results from the single factor experiments and included 17 sets of experiments. The response chosen was the yield of EMF. The values that were chosen for the variables are presented in Table 3. The central point experiment was repeated five times in order to determine the variability of the results and assess the experimental error. The experiments were conducted in random order to minimize errors resulting from possible systematic trends in the variables.

3.3.2. Model analysis. The complete experimental design matrix and responses are shown in Table 4. A multiple

regression analysis of the experimental data was performed according to the RSM, then a second-order polynomial equation was established to describe the mathematical relationship between EMF yield and the test variables based on the coded values.

$$Y = 84.48 + 1.66X_1 + 5.01X_2 + 2.40X_3 - 4.03X_1X_2 + 0.15X_1X_3 - 1.95X_2X_3 - 1.10X_1^2 - 3.15X_2^2 - 0.63X_3^2 \quad (1)$$

Y is the EMF yield, and X_1, X_2, and X_3 are the coded factors of the test variables time, temperature, and PDVTA-SO$_3$H dosage, respectively.

The values of the regression coefficients and the analysis of variance (ANOVA) of the experimental results are given in Table 5. The F-value of 83.62 and P-value lower than 0.0001 of the model imply that the model is highly significant. The lack of fit

Table 3 Independent variables and the corresponding levels

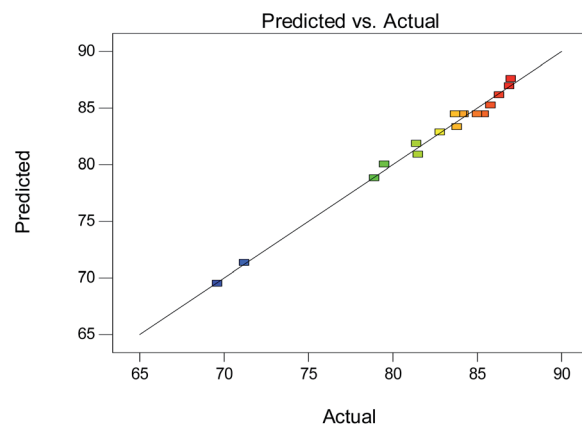| Independent variable	Units	Code	Level		
			−1	0	1
Reaction time	min	X$_1$	30	45	60
Reaction temperature	°C	X$_2$	90	100	110
Catalyst dosage	mg	X$_3$	30	40	50

Paper

Table 4 Results of the Box–Behnken design for the reaction optimisation

Entry	$t(X_1)$/min	$T(X_2)$/°C	Catalyst dosage(X_3)/mg	EMF yield/%
1	30(−1)	90(−1)	40(0)	69.6
2	60(1)	90(−1)	40(0)	81.5
3	30(−1)	110(1)	40(0)	87.0
4	60(1)	110(1)	40(0)	82.8
5	30(−1)	100(0)	30(−1)	78.9
6	60(1)	100(0)	30(−1)	81.4
7	30(−1)	100(0)	50(1)	83.8
8	60(1)	100(0)	50(1)	86.9
9	45(0)	90(−1)	30(−1)	71.2
10	45(0)	110(1)	30(−1)	85.8
11	45(0)	90(−1)	50(1)	79.5
12	45(0)	110(1)	50(1)	86.3
13	45(0)	100(0)	40(0)	84.2
14	45(0)	100(0)	40(0)	83.7
15	45(0)	100(0)	40(0)	84.1
16	45(0)	100(0)	40(0)	85.4
17	45(0)	100(0)	40(0)	85.0

Fig. 7 Relationship between predicted and experimental values for EMF yield.

was not significant, with an F-value of 1.22 and P-value of 0.4110, suggesting the model had good predictability. Moreover, the regression coefficient R^2 for the model was 0.9908, and the predicted R^2 value (0.9220) is in reasonable agreement with the adjusted value (0.9789). The signal to noise ratio is adequate for each response because the adequate precision of 32.283 is greater than 4. In addition, Fig. 7 depicts an excellent correlation between the experimental EMF yields and the predicted EMF yields obtained using the mathematical model for the entire range of values. Therefore, there is a real relationship among the selected variables, and the mathematical model can be applied to predict and analyse the conditions of the actual experiment.

Furthermore, the P-value suggests that all linear (X_1, X_2, X_3) parameters had a significant effect on the formation of EMF (P <0.05) because the P-values were as low as <0.0001. The results derived from the ANOVA demonstrated that the three individual

variables tested, reaction time, reaction temperature, and PDVTA-SO$_3$H dosage, were crucial parameters, as seen by their effects on the response variables. The first order main effect of reaction temperature (X_2) was significant, which suggests that temperature plays a crucial role in EMF production. Using the F-value, the effect of the various factors on EMF yield are reaction temperature > catalyst dosage > reaction time. To explain the interaction between the variables and determine the optimal level of maximum response for each variable, three-dimensional response surfaces and two-dimensional contour plots of the model were created, as shown in Fig. 8. Each figure presents the impact of two variables while the other factor was fixed at zero. When the catalyst dosage was lower, the yield of EMF increased with the increase of reaction temperature, but when the reaction time was longer, the EMF yield decreased with the increase of temperature. At the same time, it was also observed that the EL increased under the high temperature condition, indicating that the excessive reaction temperature will aggravate the occurrence of the side reaction, which was unfavorable to the formation of EMF.[33]

Table 5 Regression coefficients and analysis of the model for EMF yield

| Source	Sum of squares	F-value	P-value prob>F	Significance
Model	401.09	83.62	<0.0001	Significant
X_1	22.11	41.49	0.0004	
X_2	201.00	377.16	<0.0001	
X_3	46.08	86.47	<0.0001	
X_1, X_2	64.80	121.60	<0.0001	
X_1, X_3	0.090	0.17	0.6934	
X_2, X_3	15.21	28.54	0.0011	
X_1^2	5.12	9.60	0.0173	
X_2^2	41.85	78.52	<0.0001	
X_3^2	1.66	3.11	0.1211	
Lack of fit	1.78	1.22	0.4110	Not significant
R^2	0.9908			
R^2-adjusted	0.9789			
R^2-predicted	0.9220			
Adequate precision	32.383			
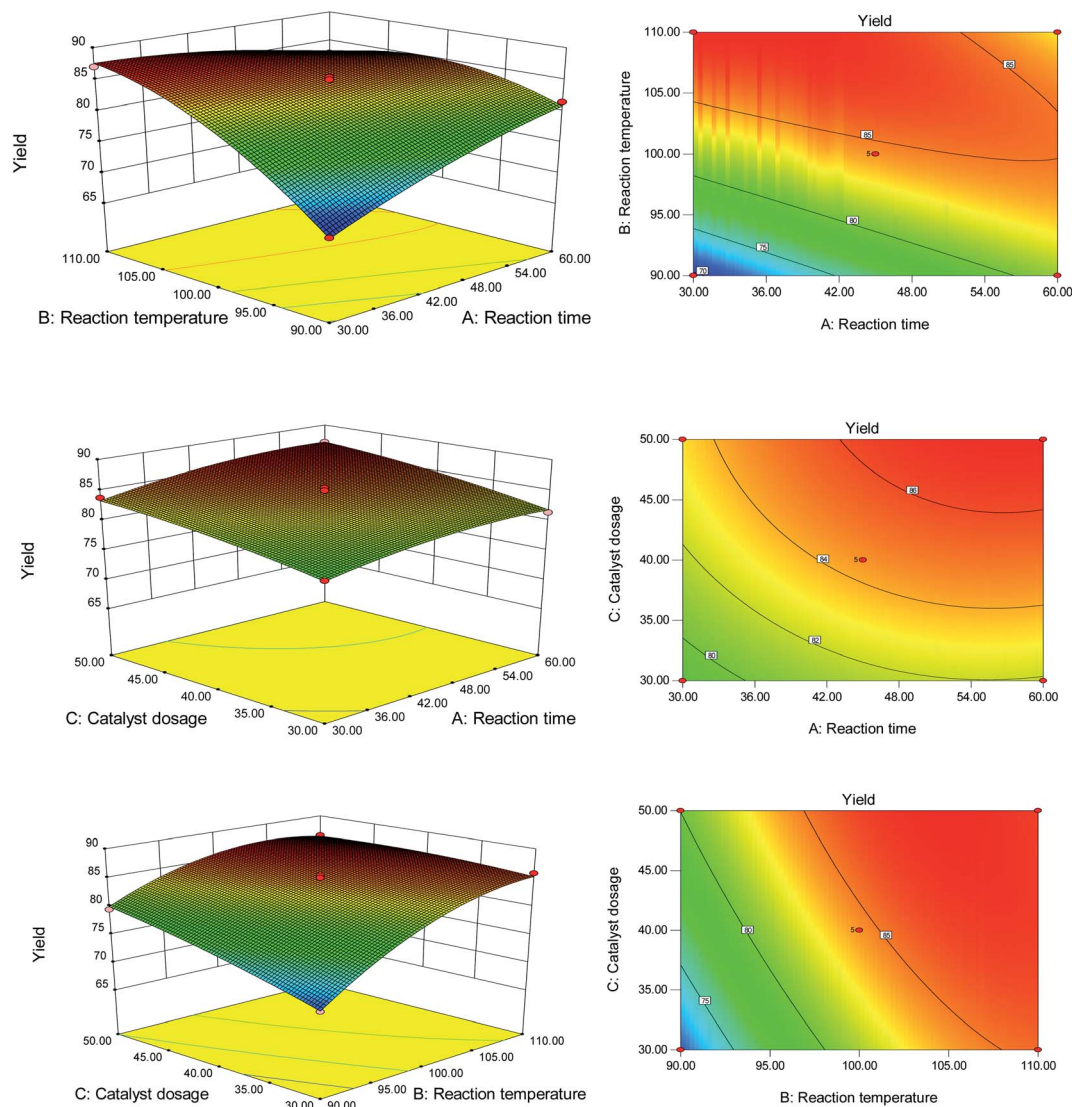
Fig. 8 3D and contour plots of EMF yield *versus* different variables.

Based on eqn (1) and using the software's numerical optimisation function, the maximum predicted EMF yield was 87.6% for the optimal conditions of a 30 min reaction time, 42.5 mg catalyst dosage, and 110 °C reaction temperature. Three experiments were carried out under the optimal conditions to verify the prediction, and an average EMF yield of 87.5% was obtained. This shows that the experimental data are in good agreement with the model, indicating that the model for the synthesis of EMF from HMF was adequate.

3.4. Catalytic etherification of HMF by different alcohols

To study the applicability of the PDVTA-SO₃H catalyst to the catalytic esterification of HMF with other alcohols, catalytic reactions were carried out using the optimised conditions described in Section 3.3. As listed in Table 6, methanol, ethanol, *n*-propanol, isopropanol, *tert*-butanol, and benzyl alcohol were used as the alcohol substrates. The product distributions indicate that HMF etherification proceeds similarly in these
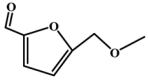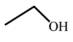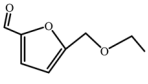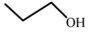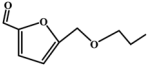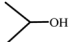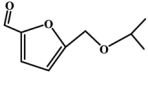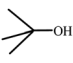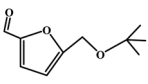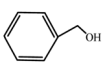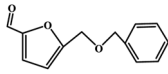
solvents, with the corresponding 5-alkoxymethylfurfural being the major product. Notably, a high yield can be obtained when using a simple alcohol, although in the case of methanol more by-products were produced at this reaction temperature than had been produced at the same temperature using ethanol, leading to lower selectivity and yield. The use of branched alcohols like isopropanol and *tert*-butanol largely delays the reaction progress, which, in association with the existing steric hindrance and possibly inadequate reaction temperature, prohibits the efficient progress of the reaction in the pore space of PDVTA-SO₃H.

3.5. Comparison of the activity with other reported catalysts

The catalytic performance of PDVTA-SO₃H is, to the best of our knowledge, better than that of other acid catalysts that have been reported for the etherification of HMF to EMF (Table 7). For example, Yuan *et al.*[34] reported that Fe₃O₄@C-SO₃H catalysed an 88.4% yield of EMF from the etherification of HMF with

Table 6 Expanded catalytic etherification experiments using different alcohols[a]

Entry	Alcohol	Ether	Yield/%
1	H_3C-OH		70.7
2			87.5
3			75.0
4			53.7
5			32.1
6			35.5

[a] Reaction conditions: 1 mmol HMF5, mL alcohol, 42.5 mg catalyst30, min, and 110 °C.

ethanol after 12 h at 100 °C. Wang et al.[35] prepared C-SO$_3$H nanomaterials from the direct pyrolysis of the metal–organic framework Cu-benzene-1,3,5-tricarboxylate (Cu-BTC) followed by acidification with sulfuric acid, and showed that the yield of EMF using this catalyst could reach a maximum of 71.0% within 6 h at 100 °C. Even though these catalytic systems gave efficient yields of EMF, still they still needed longer reaction times than reactions using the as-prepared PDVTA-SO$_3$H catalyst, which showed high yields within 30 min. The efficient catalytic activity of the PDVTA-SO$_3$H catalyst was due to the existence of an appropriate number of surface Brønsted acid sites and an appropriate pore diameter.

3.6. Catalyst recycling experiments

Reusability of heterogeneous catalysts is vital for reducing production costs in practical applications. A PDVTA-SO$_3$H recycle experiment was carried out to investigate the reusability of the catalyst under the optimal reaction conditions. The used PDVTA-SO$_3$H catalyst could be sufficiently separated from the reaction mixture by centrifugation. The catalyst was recovered, washed with ethanol three times, and dried at 60 °C before the next usage. As seen from Fig. 9, the recovered PDVTA-SO$_3$H

Table 7 Comparison of the etherification of HMF to EMF with reported different catalysts

Entry	Catalyst	T/°C	t/h	EMF yield/%	ref.
1	Fe$_3$O$_4$@C-SO$_3$H	100	12	88.4	34
2	C-SO$_3$H	100	6	71.0	35
3	PDVTA-SO$_3$H	110	0.5	87.7	This work
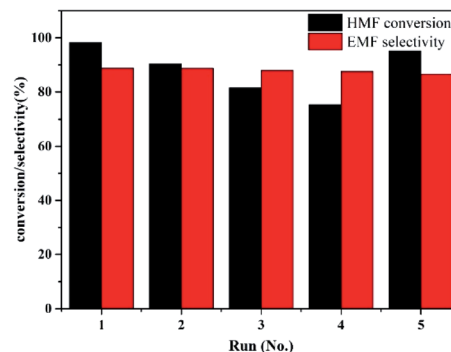
Fig. 9 Recyclability of the catalytic system.

remained catalytically active for each recycle run, although the HMF conversion decreased from 99.8% to 75.3% after four uses. The FT-IR analysis of the spent catalyst confirmed that there was no obvious structural change (Fig. 1), suggesting that the SO$_3$H groups were essentially preserved. To explore the cause of the catalyst deactivation, the amount of H$^+$ in the used catalyst after the fourth recycle run was measured by titration, and it was found that the amount of H$^+$ declined compared with the fresh catalyst (from 2.1 mmol g^{-1} to 0.9 mmol g^{-1}), indicating that the loss of catalytic activity may be a result of SO$_3$H leaching or poisoning. As further proof, the spent catalyst was analysed by elemental analysis, showing almost constant carbon content but a decrease in sulphur content by 0.4 mol g^{-1}. This suggests that functional groups might be shedding from the PDVTA-SO$_3$H. The deactivated catalyst could be easily regenerated by simple treatment in diluted HCl solution at 50 °C for 1 h, after which a HMF conversion of 95.2% was regained in a subsequent recycling experiment (Fig. 9, run 5). Therefore, the loss of catalytic activity may be due to poisoning of the SO$_3$H active sites.

4 Conclusions

EMF was efficiently synthesized from HMF by the catalyst PDVTA-SO$_3$H. The impacts of catalyst amount, temperature, and reaction time on the synthesis of EMF were further investigated in Box–Behnken design experiments based on RSM, with the model predicting a maximum EMF yield of 87.6% at 110 °C and 42.5 mg PDVTA-SO$_3$H in 30 min. The PDVTA-SO$_3$H catalyst is a promising candidate for the heterogeneous etherification of HMF to EMF and other biomass-based acid-catalysed reactions.

Conflict of interest

There are no conflicts to declare.

Acknowledgements

Notes and references

1 R. J. van Putten, J. C. van der Waal, E. De Jong, C. B. Rasrendra, H. J. Heeres and J. G. De Vries, Hydroxymethylfurfural, a versatile platform chemical made from renewable resources, *Chem. Rev.*, 2013, **113**, 1499–1597.

2 A. Bohre, S. Dutta, B. Saha and M. M. Abu-Omar, Upgrading furfurals to drop-in biofuels: an overview, *ACS Sustainable Chem. Eng.*, 2015, **3**, 1263–1277.

3 Z. Cao, Z. X. Fan, Y. Chen, M. Li, T. Shen, C. J. Zhu and H. J. Ying, Efficient preparation of 5-hydroxymethylfurfural from cellulose in a biphasic system over hafnyl phosphates, *Appl. Catal., B*, 2019, **244**, 170–177.

4 B. M. Matsagar, C. V. Nguyen, M. S. Hossain, M. T. Islam, Y. Yamauchi, P. L. Dhepe and K. C. W. Wu, Glucose isomerization catalyzed by bone char and selective production of 5-hydroxymethylfurfural in aqueous media, *Sustainable Energy Fuels*, 2018, **2**, 2148–2153.

5 L. Hu, L. Lin, Z. Wu, S. Y. Zhou and S. J. Liu, Recent advances in catalytic transformation of biomass-derived 5-hydroxymethylfurfural into the innovative fuels and chemicals, *Renewable Sustainable Energy Rev.*, 2017, **74**, 230–257.

6 S. L. Zhou, X. X. Liu, J. H. Lai, M. Zheng, W. Z. Liu, Q. Xu and D. L. Yin, Covalently linked organo-sulfonic acid modified titanate nanotube hybrid nano-structures for the catalytic esterification of levulinic acid with n-butyl alcohol, *Chem. Eng. J.*, 2019, **361**, 571–577.

7 D. W. Guo, X. X. Liu, F. Cheng, W. G. Zhao, S. Wen, Y. P. Xiang, Q. Xu, N. Y. Yu and D. L. Yin, Selective hydrogenolysis of 5-hydroxymethylfurfural to produce biofuel 2,5-dimethylfuran over Ni/ZSM-5 catalysts, *Fuel*, 2020, **274**, 117853.

8 X. Kong, Y. F. Zhu, Zh. Fang, J. A. Kozinski, I. S. Butler, L. J. Xu, H. Song and X. J. Wei, Catalytic conversion of 5-hydroxymethylfurfural to some value-added derivatives, *Green Chem.*, 2018, **20**, 3657–3682.

9 H. Li, S. Saravanamurugan, S. Yang and A. Riisager, Direct transformation of carbohydrates to the biofuel 5-ethoxymethylfurfural by solid acid catalysts, *Green Chem.*, 2014, **18**, 726–734.

10 Z. H. Wang and Q. W. Chen, Conversion of 5-hydroxymethylfurfural into 5-ethoxymethylfurfural and ethyl levulinate catalyzed by MOFs-based heteropolyacid materials, *Green Chem.*, 2016, **18**, 5884–5889.

11 S. Qureshi, E. Ahmad, K. K. Pant and S. Dutta, Insights into microwave-assisted synthesis of 5-ethoxymethylfurfural and ethyl levulinate using tungsten disulfide as catalyst, *ACS Sustainable Chem. Eng.*, 2020, **8**, 1721–1729.

12 S. Alipour, H. Omidvarborna and D. S. Kim, A review on synthesis of alkoxymethyl furfural, a biofuel candidate, *Renewable Sustainable Energy Rev.*, 2017, **71**, 908–926.

13 J. M. Wang, Z. H. Zhang, S. W. Jin and X. Z. Shen, Efficient conversion of carbohydrates into 5-hydroxylmethylfurfan and 5-ethoxymethylfurfural over sulfonic acid-functionalized mesoporous carbon catalyst, *Fuel*, 2017, **192**, 102–107.

14 J. H. Dai, Z. B. Liu, Y. X. Hu, S. Q. Liu, L. F. Chen, T. Qi, H. Q. Yang, L. F. Zhu and C. W. Hu, Adjusting the acidity of sulfonated organocatalyst for the one-pot production of 5-ethoxymethylfurfural from fructose, *Catal. Sci. Technol.*, 2019, **9**, 483–492.

15 M. Zuo, K. Le, Y. C. Feng, C. X. Xiong, Z. Li, X. H. Zeng, X. Tang, Y. Sun and L. Lin, An effective pathway for converting carbohydrates to biofuel 5-ethoxymethylfurfural via 5-hydroxymethylfurfural with deep eutectic solvents (DESs), *Ind. Crops Prod.*, 2018, **112**, 18–23.

16 H. X. Guo, A. Duereh, Y. Hiraga, T. M. Aida, X. H. Qi and R. L. Smith Jr, Perfect recycle and mechanistic role of hydrogen sulfate ionic liquids as additive in ethanol for efficient conversion of carbohydrates into 5-ethoxymethylfurfural, *Chem. Eng. J.*, 2017, **323**, 287–294.

17 G. Morales, M. Paniagua, J. A. Melero and J. Iglesias, Efficient production of 5-ethoxymethylfurfural from fructose by sulfonic mesostructured silica using DMSO as co-solvent, *Catal. Today*, 2016, **279**, 305–316.

18 P. K. Kumari, B. S. Rao, D. D. Lakshmi, N. R. S. Paramesh, C. Sumana and N. Lingaiah, Tungstophosphoric acid supported on mesoporous niobiumoxophosphate: an efficient solid acid catalyst for etherification of 5-hydroxymethylfurfural to 5-ethoxymethylfurfural, *Catal. Today*, 2018, **325**, 53–60.

19 Z. W. Wang, H. Li, Ch. J. Fang, W. F. Zhao, T. T. Yang and S. Yang, Simply assembled acidic nanospheres for efficient production of 5-ethoxymethylfurfural from 5-hydromethylfurfural and fructose, *Energy Technol.*, 2017, **5**, 2046–2054.

20 S. S. Yin, J. Sun, B. Liu and Z. H. Zhang, Magnetic material grafted cross-linked imidazolium based polyionic liquids: an efficient acid catalyst for the synthesis of promising liquid fuel 5-ethoxymethylfurfural from carbohydrates, *J. Mater. Chem. A*, 2015, **3**, 4992–4999.

21 H. X. Guo, A. Duereh, Y. Q. Su, E. J. M. Hensen, X. H. Qi and R. L. Smith Jr, Mechanistic role of protonated polar additives in ethanol for selective transformation of biomass-related compounds, *Appl. Catal., B*, 2020, **264**, 118509.

22 B. S. Rao, D. D. Lakshmi, P. K. Kumari, P. Rajitha and N. Lingaiah, Dehydrative etherification of carbohydrates to 5-ethoxymethylfurfural over SBA-15 supported Sn modified heteropoly silicate catalysts, *Sustainable Energy Fuels*, 2020, **4**, 3428–3437.

23 J. Zhang, K. J. Dong, W. M. Luo and H. F. Guan, Catalytic upgrading of carbohydrates into 5-ethoxymethylfurfural using SO$_3$H functionalized hyper-cross-linked polymer based carbonaceous materials, *Fuel*, 2018, **234**, 664–673.

24 M. Balakrishnan, E. R. Sacia and A. T. Bell, Etherification and reductive etherification of 5-(hydroxymethyl)furfural: 5-(alkoxymethyl)furfurals and 2,5-bis(alkoxymethyl)furans

as potential bio-diesel candidates, *Green Chem.*, 2012, **14**, 1626–1634.

25 R. Y. Zhong, F. Yu, W. Schutyser, Y. H. Liao, F. De Clippel, L. Peng and B. F. Sels, Acidic mesostructured silica-carbon nanocomposite catalysts for biofuels and chemicals synthesis from sugars in alcoholic solutions, *Appl. Catal., B*, 2016, **206**, 74–88.

26 Y. Y. Wen, Z. Yu, K. X. Li, H. Q. Guo, Y. H. Dai and L. S. Yan, Fabrication of biobased heterogeneous solid Brønsted acid catalysts and their application on the synthesis of liquid biofuel 5-ethoxymethylfurfural from fructose, *Green Energy Environ*, 2018, **3**, 384–391.

27 T. Chen, L. C. Peng, X. Yu and L. He, Magnetically recyclable cellulose-derived carbonaceous solid acid catalyzed the biofuel 5-ethoxymethylfurfural synthesis from renewable carbohydrates, *Fuel*, 2018, **219**, 344–352.

28 A. Kumar and R. Srivastava, FeVO$_4$ decorated –SO$_3$H functionalized polyaniline for direct conversion of sucrose to 2,5-diformylfuran & 5-ethoxymethylfurfural and selective oxidation reaction, *Mol. Catal.*, 2019, **465**, 68–79.

29 J. L. Li, Y. Q. Wang, B. Q. Lu, Y. X. Wang, T. Sh. Deng and X. L. Hou, Protonic acid catalysis of sulfonated carbon material: tunable and selective conversion of fructose in low-boiling point solvent, *Appl. Catal., A*, 2018, **566**, 140–145.

30 R. Gomes, P. Bhanja and A. Bhaumik, Sulfonated porous organic polymer as a highly efficient catalyst for the synthesis of biodiesel at room temperature, *J. Mol. Catal. A: Chem.*, 2016, **411**, 110–116.

31 F. Yang, J. Tang, R. Ou, Z. J. Guo, Sh. Y. Gao, Y. Zh. Wang, X. Y. Wang, L. Chen and A. H. Yuan, Fully catalytic upgrading synthesis of 5-Ethoxymethylfurfural from biomass-derived 5-hydroxymethylfurfural over recyclable layered-niobium-molybdate solid acid, *Appl. Catal., B*, 2019, **256**, 117786.

32 B. L. Chen, G. Zh. Xu, Zh. B. Zheng, D. X. Wang, C. H. Zou and Ch. Chang, Efficient conversion of corn stover into 5-ethoxymethylfurfural catalyzed by zeolite USY in ethanol/THF medium, *Ind. Crops Prod.*, 2019, **129**, 503–511.

33 B. L. Chen, G. Zh. Xu, Ch. Chang, Zh. B. Zheng, D. X. Wang, Sh. H. Zhang, K. Li and C. H. Zou, Efficient one-pot production of biofuel 5-ethoxymethylfurfural from corn stover: optimization and kinetics, *Energy Fuels*, 2019, **33**, 4310–4321.

34 Z. L. Yuan, Z. H. Zhang, J. D. Zheng and J. T. Lin, Efficient synthesis of promising liquid fuels 5-ethoxymethylfurfural from carbohydrates, *Fuel*, 2015, **150**, 236–242.

35 Z. H. Wang and Q. W. Chen, Variations of major product derived from conversion of 5-hydroxymethylfurfural over a modified MOFs-derived carbon material in response to reaction conditions, *Nanomaterials*, 2018, **8**, 492–500.